Experimental Verification of and Physical Interpretation for Adsorption-Dependent Squeeze-Film Damping

Yu-Jie Zhao, Gui-Lin Li, Li Liu,* Cheng-Gang Shao, Ding-Yin Tan, Hang Yin, and Ze-Bing Zhou†
MOE Key Laboratory of Fundamental Physical Quantities Measurement, Hubei Key Laboratory of Gravitation and Quantum Physics, PGMF and School of Physics, Huazhong University of Science and Technology, Wuhan, 430074, China

(Received 2 June 2022; revised 18 February 2023; accepted 23 February 2023; published 3 April 2023)

The squeeze-film-damping effect is one of the main limits in many precision experiments, especially in the study of short-range interactions, and its physical mechanism is still not very clear. We develop a torsion pendulum to measure the damping effects caused by the thermal motion of residual gas between a cubic test mass and a pair of symmetric movable plates. The measured results are consistent with the model that synthesized the elastic and inelastic collisions by introducing a thermal accommodation coefficient (TAC). In our research, the pressure dependence of the TAC, which can be expressed as an exponential decay function, is also observed. This dependence may imply that the elastic collisions correspond to the simple bouncing of residual gas molecules, while the inelastic collisions correspond to the adsorption and desorption cycle of gas molecules on the surface. The method in this work and the discovered TAC pressure dependence are instructive for the analysis of residual-gas effects in weak-force measurements, as well as the deviation correction of rarefied gas pressure measurements based on the squeeze-film-damping effect.

DOI: 10.1103/PhysRevApplied.19.044005

I. INTRODUCTION

Brownian-force noise from gas in the free molecular flow regime, which is related to viscous damping by the fluctuation-dissipation theorem, is an unavoidable noise source in the study of many weak-force measurements [1]. For example, the residual-gas effect has been considered as an important noise source for terrestrial gravitation-wave interferometers [2]. In the in-flight technical demonstration of the Laser Interferometer Space Antenna, the dominant noise in the frequency band between 1 and 10 mHz is from residual gas [3,4]. Christian [5] reviewed the theories for rarefied-gas effects in the study of an oscillating-vane vacuum gauge, and proposed a model for gas molecular damping. Zook *et al.* [6] measured the effect of residual gas in a vacuum chamber and validated Christian's model. In the study of microelectromechanical-system (MEMS) oscillators, an energy-transfer model and a model applying a differential equation of the variation in gas density were proposed and experimentally verified [7–12]. Dolesi *et al.* [13] analyzed the gas effects in gravitational-wave observatories and pointed out that the Brownian noise in a constrained volume and the squeeze-film damping in MEMS oscillators have identical physical nature. They also estimated the damping effect between a cubic test mass (TM) and a surrounding electrode housing by a torsion-pendulum experiment. The measured gas damping is consistent with the predictions of Monte Carlo simulations [14]. However, the distance between the TM and the housing cannot be adjusted in this experiment. Around the same time, distance-related gas damping was observed in a torsion pendulum consisting of a suspended plate-shaped TM and a fixed plate parallel to it [15]. The measured gas damping is smaller than the simulated gas damping, and the mismatch increases as the gap becomes smaller. Hence, the nature of the rarefied-gas effect deserves further investigation.

In theoretical studies of gas damping in a MEMS oscillator and macroscopic test body, the collision of a gas molecule on a macroscopic object is considered to be either completely elastic or completely inelastic [16,17]. To better represent actual conditions, a more-appropriate model as a combination of elastic and inelastic collisions with a thermal accommodation coefficient (TAC) σ was proposed by Maxwell [18,19]. In this model, the residual-gas-molecule collision is completely inelastic when $\sigma = 1$, and is completely elastic collision when $\sigma = 0$. On the basis of Maxwell's model, Ke *et al.* [20] proposed a more-accurate model with a TAC for an unconstrained volume and a constrained volume to evaluate gas damping in experiments on the inverse-square law [21]. In practice, the TAC is associated with many factors, such as pressure, gas composition, and surface material. At a pressure of 1 atm,

*liuli157@hust.edu.cn
†zhouzb@hust.edu.cn

TACs have been extracted from the measured slip coefficient for droplets of oil, mercury and shellac by means of the oil-drop method [22]. Apart from this, there is no other experimental report on TAC measurement, especially in rarefied gases.

To precisely evaluate the influence of Brownian noise in weak-force measurements, the theory that synthesized the elastic and inelastic collisions should be experimentally verified, and the specific TAC should be measured. For better understanding the noise sources from nonconservative disturbances on the TM in the TianQin mission [23], we perform experimental verification for the gas-damping model, and measure the TACs at different pressures with a silica-fiber-suspension torsion pendulum. From the measured results, the pressure dependence of the TAC iss observed. We suspect that the TAC of squeeze-film damping is related to the gas adsorption saturation of solid surfaces.

In this paper, we describe the experimental apparatus and the measurement method in detail in Sec. II, analyze the results and the dependence between the TAC and pressure in Sec. III, and present the conclusion in Sec. IV.

II. EXPERIMENT DESCRIPTION

A torsion pendulum is sensitive to the torque on its TM, and the effect of surrounding residual gas appears as both the TM angle fluctuation and oscillation ring down around the suspension fiber. A schematic drawing of our torsion pendulum is shown in Fig. 1(a), and the experimental setup is shown in Fig. 1(b). A hollow TM is suspended with a silica fiber, and a pair of electrodes surrounding the TM are mounted on two independent translation stages to allow the gaps between the TM and the electrodes to be adjusted.

According to the model of Ke *et al.*, the torque on a cuboid TM around the vertical axis in an infinite gas volume can be expressed as follows:

$$N_{\mathrm{rot}}^{\infty} = \sqrt{\frac{2m_0}{\pi k_B T}} p\Theta\left(a,b,c,\sigma_1\right)\dot{\theta}, \tag{1}$$

where k_B is Boltzmann's constant, T is the temperature, m_0 is the mass of a gas molecule, p is the pressure, and Θ is a coefficient that can be expressed as

$$\Theta\left(a,b,c,\sigma_1\right) = \frac{a}{3}\left(b^3+c^3\right)+\sigma_1 \times\left[\frac{abc}{4}(b+c)+\frac{bc}{12}\left(b^2+c^2\right)+\frac{\pi-4}{24}a\left(b^3+c^3\right)\right], \tag{2}$$

where a, b, and c are the height, length and width of the cuboid TM, respectively, σ_1 is the TAC in an infinite gas volume, and $\dot{\theta} = d\theta/dt$ is the angular velocity of the TM around the vertical axis.

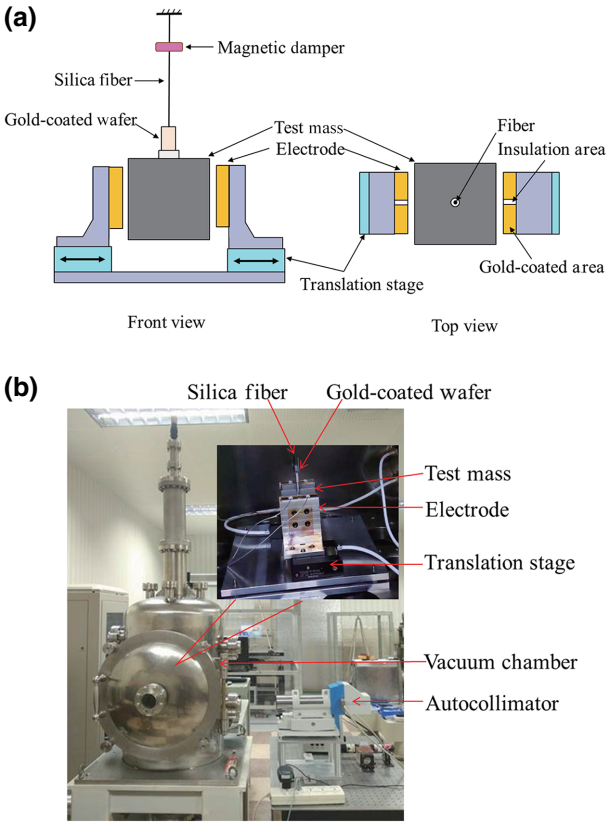

FIG. 1. (a) The torsion pendulum. A pair of electrode plates are mounted symmetrically on two independent microdisplacement translation stages beside the test mass. (b) Photographs of the experimental apparatus. The twist of the test mass is monitored by an autocollimator.

In practice, if the space around the TM is constrained, the damping force and the torque increase rapidly when the gap decreases. In detail, if a single solid plate is located parallel to and close to the side surface of the TM, the damping-torque increase on the TM around the vertical axis is expressed as

$$N_{\mathrm{rot},s} = \frac{pAR^2}{d}\frac{\tau}{1+(\omega\tau)^2}\dot{\theta}, \tag{3}$$

where A is the effective area between the plates and the TM, R is the equivalent arm length of the pendulum, d is the gap between the plate and the TM, ω is the angular frequency, and τ is the random-walk diffusion time, which can be expressed approximately as follows:

$$\tau \approx \kappa d\sqrt{\frac{\pi m_0}{2k_B T}}\frac{\sigma_2+[(1-\sigma_2)/2\pi]\left[\ln\left(1+\kappa\right)+2\right]}{\sigma_2\ln\left(1+\kappa\right)+(1-\sigma_2)\left(\sqrt{1+\kappa}-1\right)}, \tag{4}$$

where $\kappa = A/\pi d^2$ is a geometric parameter describing the area-to-gap ratio for the TM and the plates, and σ_2 is the TAC in the constrained gas volume.

From the analysis above, it can be seen that the damping torque is related to both the gap and the pressure. The damping torque on a torsion pendulum under different conditions (different gaps and pressures) can be obtained by measuring its free-amplitude attenuation, which is usually expressed as the Q factor. Therefore the TAC and its characteristics can be determined.

The TM of our torsion pendulum is a gold-coated hollow aluminum cube with edge length of 50 mm. It is suspended by a 895-mm-long and 40-μm-diameter germanium-and-bismuth-coated silica fiber from a magnetic damping stage, which is used to suppress its swing mode. To monitor the twist motion of the TM with an autocollimator, a gold-coated silica wafer with dimensions of 1.5×2.0 mm^2 is attached at the joint of the fiber and the TM. The total suspending mass and the moment of inertia are 58.6 g and 3.86×10^{-5} kg m^2, respectively.

A pair of gold-coated quartz electrode plates with side surface area of 47×47 mm^2 are symmetrically mounted parallel to the TM on two independent translation stages. The travel range of the translation stage allows the gap between the plates and the test mass can be adjusted within the range of 0–3 mm. Considering that the gaps between the test mass and the electrodes should tolerate the twist and swing motion of the torsion pendulum, the minimum gap in this experiment is set to about 0.7 mm. In addition, we think that the gap variation of 1 mm is sufficient to measure the gap dependence of damping. Therefore, the gap range is set to 0.7–1.8 mm, and a dozen gap values in this range are selected to perform the experiment. To control the twist amplitude of the TM, the coating layer of each electrode plate is divided into two isolated parts vertically, and thus electrostatic stimulation or damping torque can be applied on the TM. The torsion pendulum is installed in a vacuum chamber, whose pressure can be adjusted roughly between 10^{-5} and 10^{-2} Pa by a flapper valve between the chamber and the ion pump.

The recorded twist-angle time series of the TM are fitted to the object function of $\theta(t) = A_i \cos(2\pi ft) + A_q \sin(2\pi ft) + C$ for every three periods, and then the oscillating amplitude of each set can be obtained as $A(t) = \sqrt{A_i^2(t) + A_q^2(t)}$. Thus the Q factor of the pendulum can be determined by fitting the amplitude decay to the object function of $A(t) = A_0 e^{-\pi ft/Q}$. The period and Q factor of the torsion pendulum, when the pressure is 10^{-5} Pa and all the objects are moved about 30 cm away from the TM, are measured to be about 412 s and 14 000, respectively. Figure 2 shows the oscillation and amplitude decay of the torsion pendulum.

To reduce the influence of the electrostatic effect on the torsion pendulum, measurements are taken from two aspects. First, we measured the relation of torsion-pendulum period against the applied voltages, and obtained the stray potential on each plate part with data fitting method, then compensate it to lower than 10 mV with a high-precision source meter. Figure 3 shows the period variation and its parabolic fitting for different electrode voltages. The stray potential on each part is individually compensated. Second, the relation between the pressure in the vacuum chamber and the opening of the flapper valve is calibrated before gas-damping measurement, and thus all devices that generate charged particles, such as the vacuum gauge and the residual-gas analyzer, can be kept off during the measurement. Besides this, a charged-particle capture plate is added between the torsion pendulum and the ion pump in the vacuum chamber to avoid random charging due to ionization.

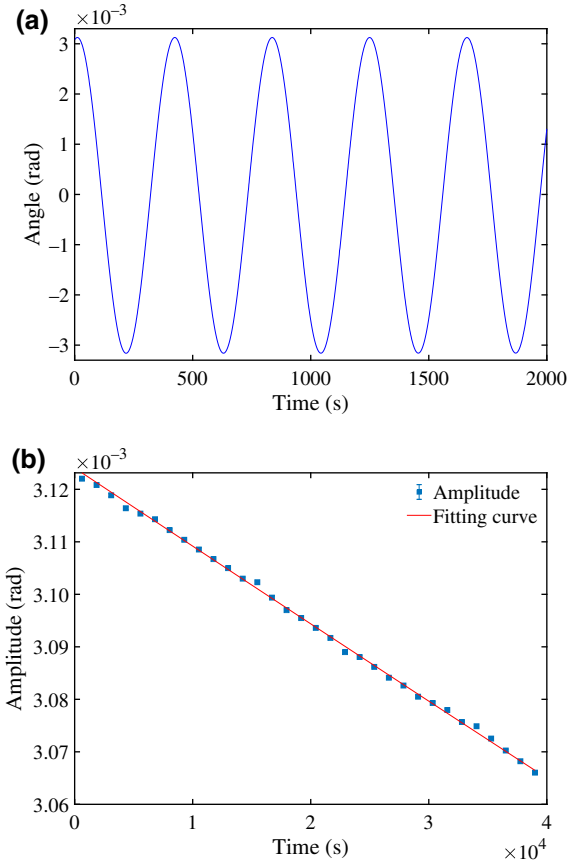

FIG. 2. Measured twist oscillation and its amplitude decay of the torsion pendulum. (a) Oscillation of the pendulum on a short timescale. (b) Amplitude decay of the torsion pendulum. The dots represent the fitting amplitudes for each cycle. The red curve is the amplitude decay fitted with an exponential decay function.

The gas-damping measurements are performed for different gaps in the range of 0.7–2.7 mm at a temperature of (296 ± 1) K, and at pressures of 2.57×10^{-4}, 2.74×10^{-3}, and 1.77×10^{-2} Pa. Under each condition, the initial amplitude of the torsion pendulum is adjusted to be about 3 mrad, and the recording for the twist angle lasted about 40 000 s. It should be noted that the measured Q factor is related to the total damping torque, including the structural

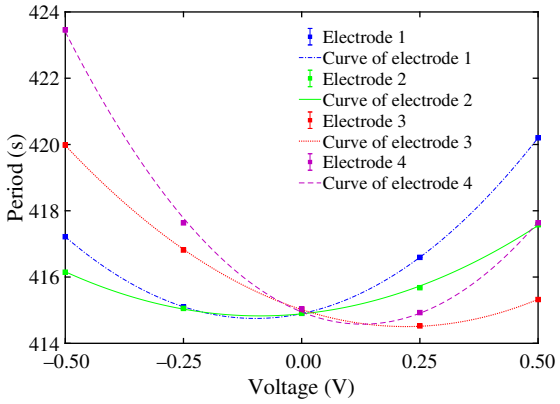

FIG. 3. Measured periods of the torsion pendulum when different voltages are applied on each electrode. Their parabolic fitting is also shown. The voltages corresponding to the lowest points of the parabolas are the stray-potential compensation voltages. It is seen that the stray potentials on different electrodes are different.

damping of the suspension fiber and the gas damping from molecule collisions. The measured Q factor, when all the objects around the TM have been removed and the pressure is 10^{-5} Pa, is treated as the background. Therefore, the damping due to gas molecules in a constrained volume (squeeze-film damping) can be expressed as the loss angle $\phi_i = 1/Q_i - 1/Q_{\rm bg}$, where Q_i is the fitted Q factor under condition i, and $Q_{\rm bg}$ is the background.

The composition of the residual gas in the chamber at different pressures is measured with a residual-gas analyzer when all the Q-factor-measurements are finished. Table I lists the main components (partial-pressure ratio) and the equivalent molecular weight of the residual gas at different pressures.

III. RESULTS AND DISCUSSION

Figure 4 shows the gap dependence of the loss angle when the pressure in the chamber is, 2.57×10^{-4}, 2.74×10^{-3}, and 1.77×10^{-2} Pa, respectively. The data points with an error bar represent the measured loss angle for different gaps. It can be seen that the loss angle is negatively related to the gap. The loss angle increases significantly when the gap decreases, showing obvious squeeze-film damping. The loss angle of the gas in an infinite volume is independent of the gap, and thus it can be treated as a constant for each condition. Since the full form of Eq. (2) is very complicated, we fit the measured data at each pressure with a numerical method based on least squares as the red curves in Fig. 4, and obtain the TACs at different pressures as 0.79 ± 0.02, 0.71 ± 0.02 and 0.53 ± 0.02 shown in Fig. 5. The theoretical curves of the loss angle versus the gap for each condition, assuming the TAC is 0 and 1, are also shown in Fig. 4, as the dashed brown line and the dot-dashed purple line. The measured loss angle at these pressures is distributed between the theoretical curves for $\sigma = 0$ and $\sigma = 1$. This indicates that the actual interaction between gas molecules and macroscopic objects includes both elastic and inelastic collision effects, which is consistent with the theoretical analysis.

Although a conductive suspension fiber is used, the release of charged particles is controlled, and the stray potential on the plates is compensated in our experiment, a residual electrostatic effect may still be present on the TM. In addition, some unmodeled effects (mainly environmental disturbance, such as tilt-twist coupling, magnetic field disturbance, and gravity gradient effect [24,25]) that introduces damping or negative damping (stimulation) may also be present on the TM, and the gap-related part of these effects will affect the TAC measurement results obtained under each condition. Therefore, the measured TAC is likely to be a biased estimation. However, these effects should not be pressure dependent, so the bias in the measured TAC do not affect the investigation of its pressure dependence.

To interpret the pressure dependence of the TAC, we suspect that the completely elastic collision is regarded as the direct collision of gas molecules with surface microscopic particles, which include the surface-constitution molecules and adsorbed gas molecules. After elastic collision, only the velocity component along the surface normal direction reversed. Additionally, the completely inelastic collision is regarded as corresponding to the molecule adsorption-desorption cycle on the solid surface. The velocity of desorbed molecules follows the cosine angular distribution, which is derived from the Maxwell-Boltzmann distribution law. If the number density of gas molecules around the object increases, more molecules are absorbed on the surface and the surface's ability to further adsorb gas molecules decreases, and so the probability of inelastic collisions decreases.

On the basis of these mechanisms, we deduce that the TAC should be larger than 0 and smaller than 1. The

TABLE I. Composition (partial-pressure ratio of main components) and equivalent moleculular weight ($\bar{A}$) of the residual gas at different pressures.

Pressure (Pa)	CO_2	CO	H_2	N_2	H_2O	$\bar{A}$ (amu)
2.57×10^{-4}	3.1%	0	18.3%	28.0%	43.8%	17.97
2.74×10^{-3}	9.6%	10.9%	20.6%	29.1%	25.1%	21.54
1.77×10^{-2}	19.2%	13.8%	15.5%	31.3%	17.6%	25.63

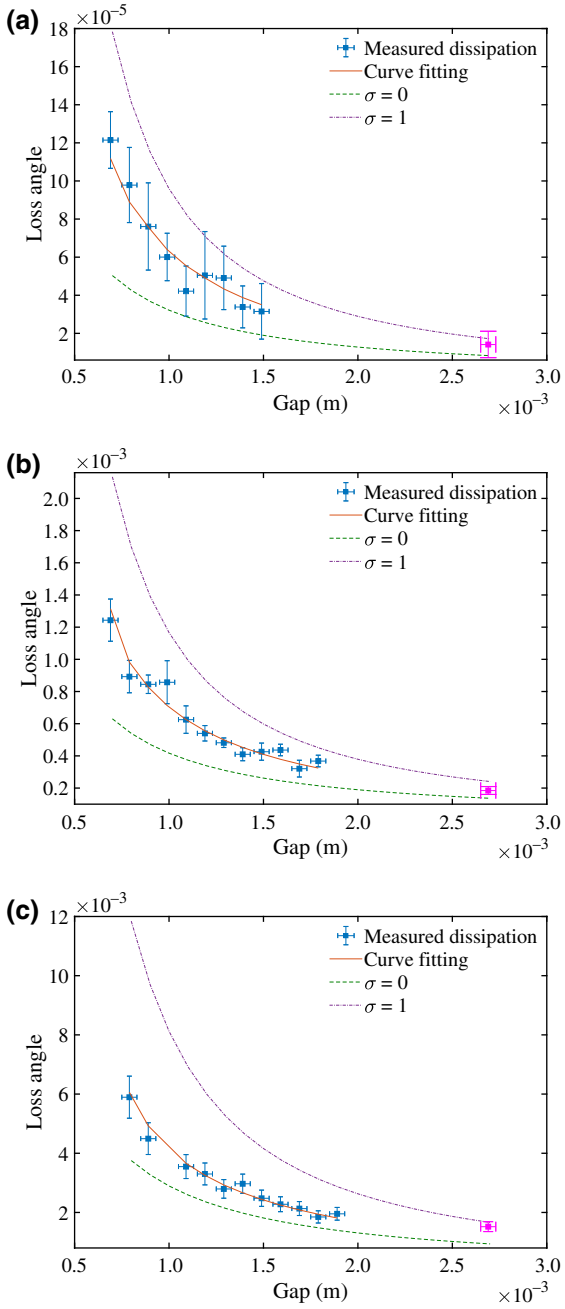

FIG. 4. Measured gap dependency of the loss angle ($\phi = 1/Q$) at different pressures: (a) the loss angle at 2.57×10^{-4} Pa; (b) the loss angle at 2.74×10^{-3} Pa; (c) the loss angle at 1.77×10^{-2} Pa. Completely inelastic collision model and completely elastic collision model predictions are also shown. The lines for $\sigma = 0$ and $\sigma = 1$ are simulated using the measured residual-gas composition. Several invalid data points (affected by misoperation, earthquakes, construction, and power outages) have been eliminated in these plots. The experimental-status-check data for each pressure are also shown as the magenta point at a gap of 2.7 mm, which is used to check the torsion-pendulum status and to verify the damping model for a big gap after the gap modulation.

reason is that elastic collision of gas molecules with the solid surface is always possible, even if no gas molecules

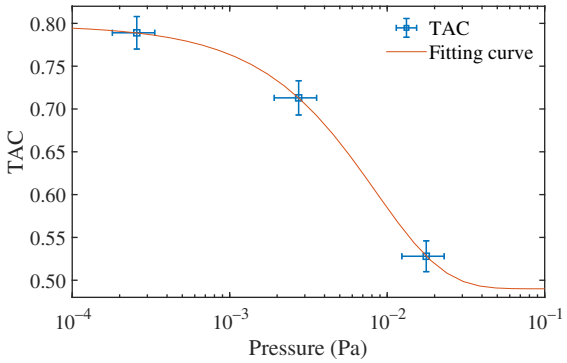

FIG. 5. TAC in squeeze-film damping as a function of residual-gas pressure. The TAC is well fitted with an exponential decay function.

are adsorbed on the surface. In addition, the free gas molecules may still be absorbed by the surface when the adsorption is saturated, because adsorption saturation is just a dynamic balance status of absorbing and desorbing. Thus, the interactions between some molecules and the adsorption-saturated surface should be still considered as inelastic collisions. The number of adsorbed molecules on the surface is proportional to the pressure (number density of molecules in the constrained volume), and the adsorption causes the pressure to decrease. Therefore, the TAC and the pressure should satisfy the following relationship:

$$\sigma = \sigma_0 e^{-\lambda p} + \sigma_\infty. \tag{5}$$

The first term is the pressure-dependent part, and the second term is the pressure independent part. $\lambda \propto \bar{d}/nk_BT$, describes the strength of the pressure dependence, where $\bar{d}$ is the mean value of the gap, and n is the maximum areal density of adsorbed molecules on the surface, which is related to the surface material and condition. The red line in Fig. 5 shows the fitting curve of the measured TAC as a function of pressure. The fitted parameters are $\sigma_0 = 0.308 \pm 0.018$, $\sigma_\infty = 0.490 \pm 0.021$, and $\lambda = (118.4 \pm 6.4)\ \mathrm{Pa}^{-1}$.

The parameters obtained with this method can be used to evaluate the adsorption and desorption characteristics of gas molecules on the surfaces of the TM and surrounding structures, which is important for further research on the outgassing properties of materials [26–29], Brownian noise, and the effect of outgassing in ultrahigh-sensitivity mechanical experiments such as the observation of gravitational waves, the experimental verification of Newton's inverse-square law at short range, and measurement of the Casimir force [30–32]. However, we must note that the obtained σ_∞ contains residual electrostatic effects due to the spatial variations of potentials on the TM and electrodes [33–36], and other damping or stimulation, so the measured TAC is just a biased estimation. The bias in the result should be investigated further in the future.

For weak-force measurements, the squeeze-film-damping effect is usually unfavorable because it greatly increases system thermal noise. But in some aspects, squeeze-film damping is beneficial for performance improvement. For example, this effect can significantly increase the damping of mechanical motion, so it helps to achieve accurate measurement of rarefied-gas pressure. The pressure sensors based on squeeze-film damping reported so far, which are designed for high pressure (greater than 0.1 Pa), have sufficient accuracy considering the effect of elastic collisions of gas molecules ($\sigma = 0$) [37–39]. However, when the gas in the test environment is very rarefied, the adsorption probability of gas molecules on the surface of the oscillator increases, so the actual TAC must be considered.

IV. CONCLUSION

In summary, we measure the gas-damping variation at different pressures and gaps in a torsion pendulum, which shows obvious squeeze-film damping. The measured damping-gap relationship verifies that the residual-gas effect on a macroscopic object is a synthesized result of two different mechanisms: elastic and inelastic collision of gas molecules. In addition, the TACs that characterize the contribution ratio of these two mechanisms under different conditions are determined in our experiment, and the TAC pressure dependence is also observed. The discovery of this dependence helps to increase the understanding of the interactions between microscopic particles and macroscopic objects. Finally, a physical explanation is given for the pressure dependence, in which the pressure affects the gas adsorption saturation of the material, and then influences the probability of inelastic collisions.

The method developed in this study is useful for the measurement of gas damping and the TAC for specific materials, spacing, and other conditions. On the one hand, the measured results can be used to guide the gas-effect analysis for weak-force measurements, and on the other hand, it can also provide a basis for TAC-related-deviation correction of rarefied gas pressure measurement based on the squeeze-film-damping effect.

ACKNOWLEDGMENTS

This work was supported by the National Key R&D Program of China (Grant No. 2020YFC2200500) and the National Natural Science Foundations of China (Grants No. 11975105, No. 11727814, and No. 12075092).

[1] P. R. Saulson, Thermal noise in mechanical experiments, Phys. Rev. D **42**, 2437 (1990).
[2] T. Uchiyama, T. Tomaru, M. E. Tobar, D. Tatsumi, S. Miyoki, M. Ohashi, K. Kuroda, T. Suzuki, N. Sato, and T. Haruyama, *et al.*, Mechanical quality factor of a cryogenic sapphire test mass for gravitational wave detectors, Phys. Lett. A **261**, 5 (1999).
[3] M. Armano, *et al.*, Sub-Femto-*g* Free Fall for Space-Based Gravitational Wave Observatories: LISA Pathfinder Results, Phys. Rev. Lett. **116**, 231101 (2016).
[4] M. Armano, *et al.*, Beyond the Required LISA Free-Fall Performance: New LISA Pathfinder Results, Phys. Rev. Lett. **120**, 061101 (2018).
[5] R. G. Christian, The theory of oscillating-vane vacuum gauges, Vacuum **16**, 175 (1966).
[6] J. D. Zook, D. W. Burns, H. Guckel, J. J. Sniegowski, R. L. Engelstad, and Z. Feng, Characteristics of polysilicon resonant microbeams, Sens. Actuators A **35**, 51 (1992).
[7] M. H. Bao, H. Yang, H. Yin, and Y. C. Sun, Energy transfer model for squeeze-film air damping in low vacuum, J. Micromech. Microeng. **12**, 341 (2002).
[8] S. Hutcherson and W. Ye, On the squeeze-film damping of micro-resonators in the free-molecule regime, J. Micromech. Microeng. **14**, 1726 (2004).
[9] G. Hong and W. Ye, A macromodel for squeeze-film air damping in the free-molecule regime, Phys. Fluids **22**, 012001 (2010).
[10] C. H. Lu, P. Li, M. H. Bao, and Y. M. Fang, A generalized energy transfer model for squeeze-film air damping in the free molecular regime, J. Micromech. Microeng. **28**, 085003 (2018).
[11] H. Sumali, Squeeze-film damping in the free molecular regime: Model validation and measurement on a MEMS, J. Micromech. Microeng. **17**, 2231 (2007).
[12] P. Li and R. F. Hu, A model for squeeze-film damping of perforated MEMS devices in the free molecular regime, J. Micromech. Microeng. **21**, 025006 (2011).
[13] R. Dolesi, M. Hueller, D. Nicolodi, D. Tombolato, S. Vitale, P. J. Wass, W. J. Weber, M. Evans, P. Fritschel, R. Weiss, *et al.*, Brownian force noise from molecular collisions and the sensitivity of advanced gravitational wave observatories, Phy. Rev. D **84**, 063007 (2011).
[14] A. Cavalleri, *et al.*, Increased Brownian Force Noise from Molecular Impacts in a Constrained Volume, Phy. Rev. Lett. **103**, 140601 (2009).
[15] S. Schlamminger, C. A. Hagedorn, and J. H. Gundlach, Indirect evidence for Lévy walks in squeeze film damping, Phy. Rev. D **81**, 123008 (2010).
[16] M. A. G. Suijlen, J. J. Koning, M. A. J. V. Gils, and H. C. W. Beijerinck, Squeeze film damping in the free molecular flow regime with full thermal accommodation, Sens. Actuators A **156**, 171 (2009).
[17] A. Cavalleri, G. Giani, R. Dolesi, D. Nicolodi, D. Tombolato, S. Vitale, P. J. Wass, and W. J. Weber, Gas damping force noise on a macroscopic test body in an infinite gas reservoir, Phys. Lett. A **374**, 3365 (2010).
[18] W. D. Niven and J. C. Maxwell, The Scientific Papers of James Clerk Maxwell (Cambridge University Press, Cambridge, United Kingdom, 1890), Vol. 2.
[19] C. Shen, *Rarefied Gas Dynamics*, Fundamentals, Simulations and Micro Flows (Springer, Berlin, 2005).
[20] J. Ke, J. Luo, Y. J. Tan, and C. G. Shao, Influence of the residual gas damping noise in the test of the gravitational inverse-square law, Classical Quantum Gravity **37**, 205008 (2020).

[21] W. H. Tan, A. B. Du, W. C. Dong, S. Q. Yang, C. G. Shao, S. G. Guan, Q. L. Wang, B. F. Zhan, P. S. Luo, and L. C. Tu, *et al.*, Improvement for Testing the Gravitational Inverse-Square Law at the Submillimeter Range, Phys. Rev. Lett. **124**, 051301 (2020).
[22] R. A. Millikan, Coefficients of slip in gases and the law of reflection of molecules from the surfaces of solids and liquids, Phys. Rev. **21**, 3 (1923).
[23] J. Luo, *et al.*, TianQin: A space-borne gravitational wave detector, Classical Quantum Gravity **33**, 035010 (2016).
[24] L. Carbone1, A. Cavalleri, R. Dolesi, C. D. Hoyle, M. Hueller, S. Vitale, and W. J. Weber, Upper limits on stray force noise for LISA, Classical Quantum Gravity **21**, S611 (2004).
[25] G. L. Smith, C. D. Hoyle, J. H. Gundlach, E. G. Adelberger, B. R. Heckel, and H. E. Swanson, Short-range tests of the equivalence principle, Phys. Rev. D **61**, 022001 (1999).
[26] Z. W. Gortel, H. J. Kreuzer, R. Teshima, and L. A. Tursk, Kinetic equations for desorption, Phys. Rev. B **24**, 4456 (1981).
[27] M. Moraw, Analysis of outgassing characteristics of metals, Vacuum **36**, 523 (1986).
[28] A. Raukema and A. W. Kleyn, Transient Trapping Desorption of Molecules at Surfaces, Phys. Rev. Lett. **74**, 4333 (1995).
[29] S. J. Manzi, R. E. Belardinelli, G. Costanza, and V. D. Pereyra, Additional constraints in adsorption-desorption kinetics, Phys. Rev. E **79**, 021103 (2009).
[30] L. Carbone, A. Cavalleri, G. Ciani, R. Dolesi, M. Hueller, D. Tombolato, S. Vitale, and W. J. Weber, Thermal gradient-induced forces on geodesic reference masses for LISA, Phys. Rev. D **76**, 102003 (2007).
[31] J. Ke, J. Luo, Y. J. Tan, Z. Liu, C. G. Shao, and S. Q. Yang, Non-isothermal squeeze film damping in the test of gravitational inverse-square law, Classical Quantum Gravity **39**, 115004 (2022).
[32] S. K. Lamoreaux, The Casimir force: Background, experiments, and applications, Rep. Prog. Phys. **68**, 201 (2005).
[33] C. C. Speake and C. Trenkel, Forces between Conducting Surfaces due to Spatial Variations of Surface Potential, Phys. Rev. Lett. **90**, 160403 (2003).
[34] W. J. Kim, A. O. Sushkov, D. A. R. Dalvit, and S. K. Lamoreaux, Surface contact potential patches and Casimir force measurements, Phys. Rev. A **81**, 022505 (2010).
[35] R. O. Behunin, D. A. R. Dalvit, R. S. Decca, and C. C. Speake, Limits on the accuracy of force sensing at short separations due to patch potentials, Phys. Rev. D **89**, 051301(R) (2014).
[36] H. Yin, Y. Z. Bai, M. Hu, L. Liu, J. Luo, D. Y. Tan, H. C. Yeh, and Z. B. Zhou, Measurements of temporal and spatial variation of surface potential using a torsion pendulum and a scanning conducting probe, Phys. Rev. D **90**, 122001 (2014).
[37] S. Naserbakht and A. Dantan, Squeeze film pressure sensors based on SiN membrane sandwiches, Sens. Actuators A **298**, 111588 (2019).
[38] A. Dantan, Membrane sandwich squeeze film pressure sensors, J. Appl. Phys. **128**, 091101 (2020).
[39] L. Mol, L. A. Rocha, E. Cretu, and R. F. Wolffenbuttel, in *Proceedings of IMECE2006*, p. 14451. (Chicago, USA, 2006).